Journal of Neurology & Neuropsychiatry

Volume 2 Issue 1, June 2025

Article

Transit Phases and beta amyloid aggregation/clearance in Al-induced Alzheimer's' disease in rat brain hippocampus: Synchrotron Fourier transform infrared microspectroscopy (SFTIRM) Study

Safaa K. H. Khalil [1], W. El Hotaby [1], Gehan A.-R. Ahmed [1,*], Gihan Kamel [2,3], Hadeer H.A. Sherif [1], Lamyaa Abbas [1]

[1] Spectroscopy Dept., Physics Research Institute, National Research Centre, 33 El Bohouth St. (former El Tahrir St.), Dokki, Giza, Egypt, P.O. 12622
[2] SESAME (Synchrotron Light for Experimental Science and Applications in the Middle East), Jordan
[3] Department of Physics, Faculty of Science, Helwan University, Cairo, Egypt
* Correspondence: Gehan A.-R. Ahmed; Spectroscopy Dept., Physics Research Institute, National Research Centre, 33 El Bohouth St. (former El Tahrir St.), Dokki, Giza, Egypt

Abstract

Background: Protein misfolding and beta amyloid (A) aggregation can induce Alzheimer's disease (AD)-like by Aluminium (Al) in rat hippocampal brain tissue. Al can produce free radicals, trigger membrane peroxidation and protein oxidation disrupt acetylcholine content leading to synaptic loss, neural death and cognitive dysfunction symptoms that are strongly associated with AD pathogenesis. Medicinal plant Lepedium sativum (LS) water extract proved promising curative effects and its ability to restore the protein integrity, with a marked clearing of A that was reported in our previous reports. Methods: In this study we utilized Synchrotron Fourier Transform Infrared Microspectroscopy (SFTIRM) and multivariate analysis to investigate and monitor more thoroughly the process of protein misfolding in response to Al and curative effect of LS treatment as well. Results: The results revealed a marked increase in the protein -structure in AD group after 42d of AL intoxication over the random coil structure. Thus, suggesting two transit phases of A formation. Meanwhile, at late stage of Al neurotoxicity after 65d 91% of the amide I is random coil and the rest is anti-parallel -sheets, alpha helix structure is absent in both tested times too. Incredibly, this random coil structure is totally absent in the curative group; instead, it is dominated by a drastic increase in the protein structure suggesting the clearance of A takes place through -structure transit phase. The role of –structure random coil as a transit phase in transformation of A and/or clearance in response to AL and LS treatment after at 42d 65d respectively is supported by different calculated % area ratio measurements as well. Conclusions: LS treatment strongly proved its reversed action on A misfolding that helped to restore the hippocampal protein integrities. SFTIRM gave unique and deeper cluster of data over the conventional FTIR in studying hippocampal brain tissue.

Keywords: Alzheimer's disease ; Protein misfolding ; hippocampal; SFTIRM; Multivariate analysis

Received: 14-08-2024
Accepted: 16-09-2024
Published: 21-06-2025

1. Introduction

It is well known that the misfolding of proteins and the formation of beta-amyloids $(A\beta)$ [Amyloidosis] and oxidative stress (OS) are considered the main reasons of many diseases, such as Alzheimer's disease (AD, Parkinson's disease, diabetes mellitus, etc. [1–5].

A living cell loses its function as a specific protein requires a distinct conformational structure to perform its role [6]. Alzheimer's disease (AD), as a neurodegenerative disorder, is a typical characteristic form of amyloidosis [3–5,7]. The β-secretase enzyme at the membrane surface cleaves the amyloid precursor protein (APP), resulting in the production of Aβ [8,9].

The pathological hallmarks of AD begin with unusual extracellular soluble Aβ deposition, followed by highly phosphorylated processes that lead to the transformation of Aβ through oligomeric intermediate phases into hard, insoluble neurofibrillary tangles (NFTs). These proteins form intracellularly and are known as tau proteins or plaques in hippocampal and cortical brain tissues [3,10–13]. Soluble Aβ (90% of Aβ is 40 amino acids long) and insoluble hydrophobic NFTs (10% of Aβ is 42 amino acids long) are neurotoxic and cause synaptic loss, neuronal death, and brain inflammation [1,8,14,15].

Aluminium (Al) is well known as a neurotoxic agent that promotes the production of soluble Aβ and insoluble NFTs associated with AD pathogenesis, due to its high affinity for membrane phospholipids and proteins [3,5,14,16].

AD has no cure; no efficient or promising therapy has yet reached the market [3,15]. Existing treatments aim to increase acetylcholine (ACh) concentration in the synaptic cleft through acetylcholinesterase inhibitors and anti–Aβ vaccines. However, these drugs demonstrate liver toxicity, modest therapeutic benefit, and do not prevent continuous misfolded protein formation, synaptic dysfunction, memory deterioration, and behavioural decline [17–20].

Despite advancements in synthetic drug development, medicinal plants remain an important source of therapeutics [21]. Herbal medications are preferred for their safety profiles and fewer side effects [22]. The pharmacological activity and medical uses of Lepidium sativum (LS) have been reported in both rat models and humans [21–23].

[23] investigated LS seeds and reported that they contain volatile essential oils, fatty oils, carbohydrates, proteins, fatty acids, amino acids, vitamins (including β-carotene, riboflavin, niacin, and ascorbic acid), flavonoids, and glycosides, along with imidazole alkaloids and essential oils.

Moreover, LS contains several active ingredients relevant to AD management: 1) **Natural antioxidants** — high lipid content, low antioxidant concentration, and high oxygen turnover make the brain susceptible to ROS damage mediated by Al, leading to oxidative stress and AD-like pathology [24]. ROS can cause lipid peroxidation, ATPase inhibition, protein oxidation, and redox modulation of ion channels [25]. LS acts as a radical scavenger, reducing oxidative stress damage. 2) **Silicon (Si)** — a metal chelator that reduces AD risk and protects cognitive function. It decreases Al absorption in the digestive tract, lowering its accumulation in the brain [26,27]. 3) **Sinapic acid** — exerts antioxidant, antimicrobial, anti-inflammatory, anticancer, and anxiolytic effects [28–30]. Its derivative, sinapine (sinapoyl choline), functions as an acetylcholinesterase inhibitor, offering therapeutic potential in AD.

Several studies report the therapeutic benefits of LS in AD-like rat models at hippocampal and cortical levels using conventional FTIR spectroscopy. LS reduces brain atrophy and hydrocephalus, observed via FTIR, MRI, histopathology, EPR, and behavioural assessments [3,5,16].

Synchrotron FTIR microscopy (SFTIRM) with chemical mapping enables highly accurate biochemical profiling of biological samples, including protein secondary structures

such as α-helix, β-sheet, and random coils within the amide I band (1600–1700 cm^{-1}) [31–33]. SFTIRM is 100–1000 times brighter than conventional thermal sources [30]. The high flux density dramatically improves the S/N ratio over very small regions [34,35].

The aim of this study is to utilize SFTIRM to detail how misfolded proteins and Aβ formation occur during Al induction in rat hippocampal tissue, and to investigate the therapeutic action of LS in reversing misfolding through transitional phases.

A previous ATR-IR study by the author on $AlCl_3$-induced AD demonstrated LS-mediated protective and curative effects, suggesting potential pathways of protein misfolding reversal. The current SFTIRM approach aims to provide high-resolution mechanistic details of Al toxicity and LS treatment effects in the rat brain hippocampus.

2. Materials and Methods

2.1. Animals & Experimental Design:

Twenty-four Albino Wister male rats weighing between 120 to 140 g were used for this study. Animals were grouped randomly in cages, the humidity, the temperature, the exposure to light and dark were applied as described in full details in our previous work [16]. All applicable international, national and/or institutional guidelines for the care and use of animals were followed. This study was approved by Experimental Animal Research and Ethics Committee, NRC, Cairo; NRC ethical approval (17 038- FWA 00014747). All methods are reported in accordance with ARRIVE guidelines. Rats were allowed to acclimatize to the laboratory environment for one week before the experiment [3,5,14,16]. All rats received the same basic diet during the experimental period (65 days). Diet and water supplied ad-libitum.

2.1.1. Animals' Groups:

Four groups of rats (n=6 rats) were divided randomly as follows: 1- Control group (Cont): these rats were injected with normal saline intra-peritoneal (i.p.) and given normal saline by oral gavage during the experimental period. 2- AD-induced group (AD): rats were injected i.p with AlCl3 dissolved in distilled water (10 mg/kg of body weight) daily and were given normal saline by oral gavage (Li et al., 2012). 3- Curative group (Cur): rats were injected i.p with AlCl3 dissolved in distilled water for the whole experimental period (10 mg/kg of body weight) daily, and are given normal saline by oral gavage for the first 3 weeks (to insure the development of AD-like pathogenesis) and then switched to LS water extract (20 mg/kg) via oral gavage daily for the rest of the experiment [3]. 4- Sham group (LS): rats were i.p injected with normal saline daily and were given LS water extract (20 mg/kg) via oral gavage daily throughout the duration of the experiment.

2.1.2. Preparation of Lepedium sativum aqueous extract

LS seeds were purchased from a local market and the aqueous extract was prepared according to the Moroccan traditional phytotherapy [4,37]. The aqueous extract was filtered using a Millipore filter (Millipore 0.2 mm, St Quentin en Yvelines, France). The filtrate was then freeze-dried and the desired dose (20 mg of lyophilized aqueous extract of LS seeds per kg body weight) was then prepared and reconstituted in 0.5 ml of distilled water. The aqueous extracts were reconstituted daily, just before administration. This method is described in full details in our previous work (Ahmed et al. 2020b, a).

2.1.3. Brain tissue sections for SFTIRM measurement

At the desired time interval and overnight fasting, the rats were sacrificed by cervical dislocation at the end of 42d and 65d. The whole brain of each rat (3 from each group) rapidly and carefully removed from the skull. The isolated hippocampal brain tissues were

quickly fixed in 4% buffered formaldehyde and embedded in paraffin according to routine tissue processing for pathological examination [3,5,14,16]. For each sample, 5-m-thick sections were cut and deposited on Mirr-IR slides for SFTIRM mapping studies. Tissue slides were de-waxed by immersing them in xylene for 5min and repeating this step twice with fresh xylene. The slides then were immersed in 100% ethanol for another 5min and allowed to dry in air at room temperature according to [38].

2.1.4. Synchrotron-FTIRM Measurements

SFTIRM data were collected at the IR beamline of SESAME (Synchrotron light for Experimental Science and Applications in the Middle East) light source, Jordan. For the microspectroscopy beamline the beam is directed to a Nicolet Continuum IR microscope (Thermo Fisher Scientific©, USA) equipped with a liquid-nitrogen-cooled mercurycadmium-telluride (MCT) detector [3,5,14,16]. The Continuum microscope is coupled to 8700 Thermo Spectrometer and the data collection was carried out using Thermo OMNIC software. Mapping was performed with Atlus mapping software (Thermo Fisher Scientific, USA). The microscope and the spectrometer are purged with dry air to minimize water vapour and carbon dioxide interference with the spectra. Samples' sections were fixed on MirrIR slides (Kevley Technologies, UK) and consequently mounted on Prior scan motorized stage for data collection. Background spectra of tissue free region were collected before each map to assess its contribution. 128 Spectra were recorded in reflection mode in the region 4000–650 cm1 with a spectral resolution of 4 cm1 using an aperture of 20×20µm2. Area maps were collected with 10 µm step size increment (approximately 42 spectra collected per map and the degree of freedom was between 3327). Each spectrum was baseline corrected in the 4000-650 cm-1 normalized the entire spectrum to the absorbance of amide I (around 1654 cm1 by using OMNIC 8.3 software program (Thermo Fisher Scientific Inc., Massachusetts, USA). To increase the resolution of the overlapping bands before any measurements, a Gaussian decomposition was used to localize the position of the bands in the spectra over the amide I and amide II bands over the range (1700-1500cm-1) by using the same software (baseline taken 1718-1477cm-1). Second derivative analysis was carried by using Savitzky-Golay filter with selected 9 point of smoothing with the same software.

2.1.5. Statistical analysis

The spectral differences among the groups under investigation were determined using multivariate exploratory techniques; Principal component analysis (PCA) and Hierarchical cluster analysis (HCA), exactly as described before in (Ahmed et al. 2020b, a).The multivariate classification (data recognition) was performed on the previously processed SFTIRM collected spectra between the intensities of the IR bands over the amide I and amide II bands.

3. Results & Discussion

In this study we applied SFTIRM to screen out the protein misfolding in rat hippocampal tissue in response to both Al toxicity and the influence of LS in reversing these protein misfolding as proved earlier [3,5,14,16] over the amide I and amide II range [1700-1500cm-1] This section may be divided by subheadings. It should provide a concise and precise description of the experimental results, their interpretation as well as the experimental conclusions that can be drawn.

- SFTIRM spectra
- Second derivative analysis

Very slight changes are observed from the raw spectra obtained from Cont, AD, Cur and LS groups; the spectra are nearly superimposed (data not shown). For deeper spectral

analysis, spectral second derivative and curve fitting were carried over the selected amide I & II regions from the computed averaged, normalized, smoothed and baseline corrected spectra obtained from each group. Figure 1 illustrated the second derivatives of Cont, AD, Cur, and LS groups at the two tested time intervals [42d, 65d] respectively. The amide I band arises mainly to carbonyl C=O stretching vibrational modes of proteins, while the amide II band is due to N–H bending and C–N stretching of proteins [39–44]. Only the marked changes in the amide II second derivatives bands are noticed in the early stage of the experiment at 42d Figure 1

It seems that, at early stage of treatment [42d] the noticed spectral changes in the hippocampal proteins secondary structure beginning mainly in the NH bending of proteins i.e. in the amide II bands Fig (1a). This may be referred to the fact that, along the process of proteins aggregation, peptide bonds are formed between the NH2 and C=O of the amino acids as they both strongly contribute to this process. Meanwhile, the most significant spectral changes in band intensities, HBW, bands position, disappearance and appearance of new bands are clearly shown in AD group at 65d rather than the Cont and the other LS treated groups [Cur & LS] for both the amide I and amide II bands] Fig (1b). This is logic, because as the time and the process of misfolding proteins and aggregation increase it should be accompanied by a dramatic alteration in the SFTIRM spectra. Figure 1 revealed a very broad wide amide I band in AD 2nd der. spectrum centred at 1643 cm-1 with doublet in the amide II band at 15331546 cm-1 , that were shifted to lower frequency, and appearance of a new band at1585 cm-1 compared to the Cont 2nd der. spectrum

[Figure 1 lack arrows]. Cur spectrum showed several small bands in the amide II region compared to the AD 2nd der. spectrum [Fig (1b) black stars]. It is also obvious from Fig (1b) that the C=O stretching carbonyl bands in the AD group are depleted than the Cont and the other LS tested groups [black arrow]. This observation agrees with Catherine et al., [45] who stated the disappearance of the lipid carbonyl band at 1738 cm-1 in the SFTIR spectrum of Aβ42, aggregated plaque.

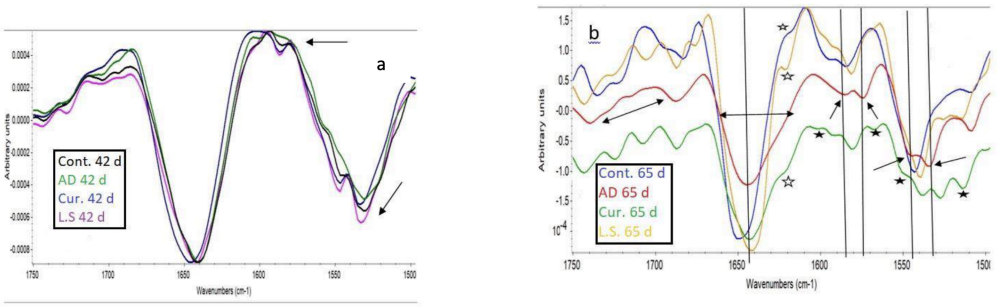

42d hippo 65d hippo

Figure 1. (A) SFTIRM normalised, mean second derivative spectra from Cont, AD, Curative and LS groups over the amide I and amide II region. (**a**) After 42days, there are marked alteration in the in AD 2nd der compared to the other tested groups specifically for the amide II region (black arrows). . (B) Normalised, mean second derivative SFTIRM spectra from Cont, AD, Curative and LS groups over the amide I and amide II region After 65d, the black arrows pointed to the substantial changes in the AD 2nd der spectrum for both amide I and amide II compared to the control and the other LS tested groups [Cur & LS]. The depletion of the carbonyl C=O stretching bands is observed. The intensity, HBW and the position of the amide modes are both affected by Al and LS treatment.

3.1. Curve Fitting Analysis

For more qualitative and quantitative spectral analysis, curve fitting of the amide I & II region over 1700-1500 cm-1 were carried from the previously protein processed map (Fig. S1). We choose the darkest red-hot spectrum/spectra from each map, the resolved amide I

and amide II sub-bands, the band position, the HBW and the percentage area are given in (Table 1) together with their corresponding band assignments. It is clear from (Table 1) that at 42d of treatment, for the amide I, which is usually used to give all details about the protein secondary structure as C=O stretching vibrational mode is greatly affected by the hydrogen bonds between -helix, β-sheets, random coil, and β-turn structure [46,47]. Its sub-band around 1640 cm-1 detected in the Cont. peak resolved spectrum/spectra is shifted to higher wavenumber around 1645-1642 cm-1 in the AD group. This band is mainly arisen from the C=O stretching mode of vibration of proteins and is due to random coil secondary structure. It should be mentioned here that, the two different spectra taken for the curve fitting from AD [AD1, AD2] group gave two obviously different sub-bands. These is evident by the results obtained from both HCA and PCA [that will be discussed here later]. It seems that at early stage of Al intoxication, we have two different protein secondary structure; one is closely like the control while, the other is completely different.

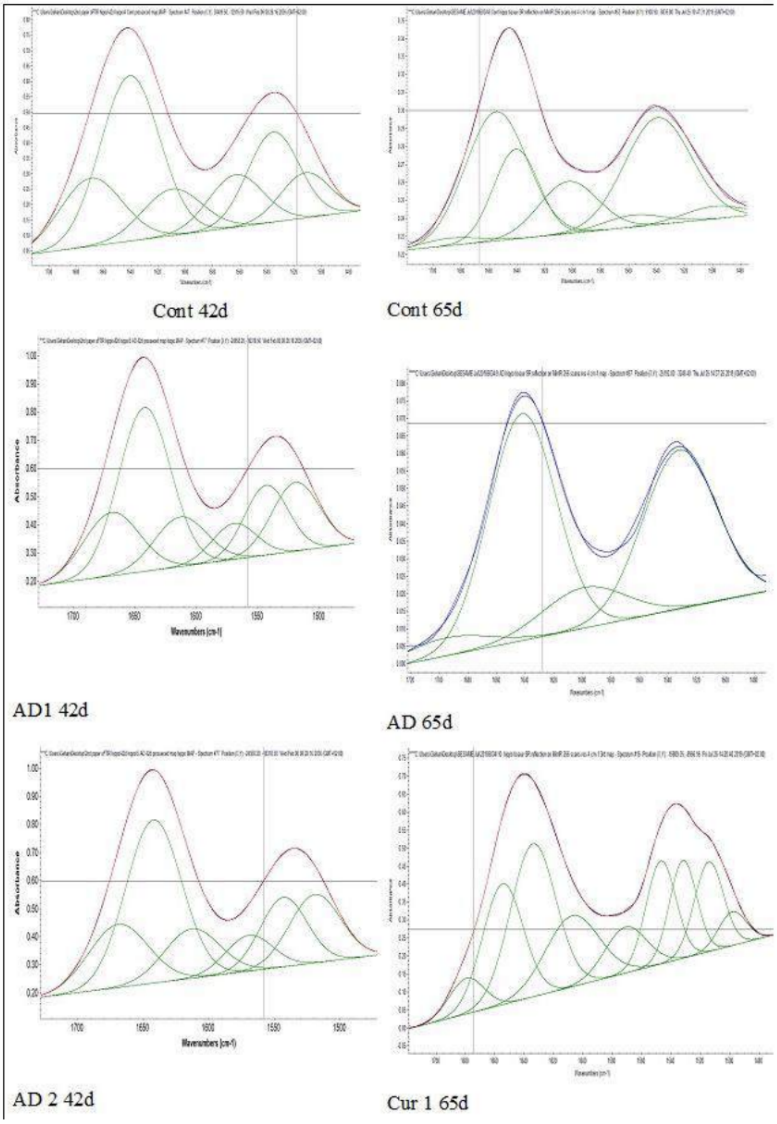

Figure S1. SFTIRM curve-fitted spectra of amide I and II bands.

In addition to the noticed band shift, the appearance of a new bands in both AD1curve fitted spectrum around 1621, 1677 cm-1 is also detected which correspond to β-turns and parallel β-sheets secondary structure respectively. This result Consistent with Lisa et al., 2006 [34] findings that detected an elevated β-sheet secondary structure in amyloid plaques

indicated by the strong absorbance SFTIR band at 1625 cm-1 compared to other surrounded unaffected area. β-sheets secondary structure as a shoulder of the dense core plaque at 1630 cm-1 was also recorded [48]. However, the protein secondary structure may contain another type of protein secondary structure. Many reports showed a conflicting view about the structure of tau proteins in AD brain, as it may be mainly -helical structure to mainly β-sheet, or a mixture of mostly random coil and increased amount of β- structure [49–51]. In our study, the hippocampal tissue at 42d for all groups are dominated with random coil, the band around 1640 cm-1, over β-sheet structure respectively. On the other hand, the amide II sub-bands have nearly the same values in AD1 as the control group, but in AD2 they have marked bands shift towards higher frequencies than the control curve fitted group [Table1] [from 1511, 1535, 1562 cm-1 to 1518, 1542,1569 cm-1] respectively. It may be suggested that the beginning of misfolded proteins starts in the NH bending functional groups evident by the recorded increase in amide II sub-bands HBW in AD group compared to the control [Table 1]. This observation holds true for the curative group at 42d. By contrast, in LS treated groups, Cur & LS spectral analysis, showed nearly the same amide I sub-band with around 1610 cm-1, 1621 cm-1 respectively with the appearance of new band around 1671 cm-1, that corresponds to β-sheet structure, and a band shift to higher frequency at 1645 , 1642 cm-1 for Cur & LS curve fitting data respectively.

Table 1. The sub-bands positions, HBW and percentage areas, of amide I sub-bands (1700–1500 cm1) of the rat brain hippocampal tissue for control, AL, Curative (Cur) and LS treated groups at 42d 65 days.

Control			AD Group						Cur.			L.S		
			AD1			AD2								
Center X	FWHH	% Area	Center X	FWHH	% Area	Center X	FWHH	% Area	Center X	FWHH	% Area	Center X	FWHH	% Area
1511.56	42.87	8.48	1511.62	43.18	7.80	1518.93	45.56	14.54	1529.278	53.209	15.6125	1521.736	48.855	16.7764
1535.19	44.40	17.51	1534.79	45.46	17.51	1542.89	41.7	13.51	1557.638	54.397	10.7216	1545.96	46.489	15.8532
1562.69	46.72	10.70	1561.83	48.41	9.73	1569.10	41.683	6.96	1610.975	53.076	6.4267	1571.473	44.751	5.8666
1609.60	50.98	10.36	1621.24	58.59	17.65	1612.83	49.655	11.43	1644.521	52.026	29.6072	1612.969	50.314	9.3758
1640.59	51.08	36.979	1645.94	52.88	39.49	1642.06	49.91	37.93	1671.494	50.92	8.7129	1642.395	51.538	37.0312
1669.15	53.468	15.94	1676.95	50.20	7.79	1668.83	53.04	15.60	–	–	–	1671.334	54.021	15.0965

Control			AD1			Curative Group						L.S		
						Cur.1			Cur.2					
Center X	FWHH	% Area	Center X	FWHH	% Area	Center X	FWHH	% Area	Center X	FWHH	% Area	Center X	FWHH	% Area
1538.954	55.966	3.5489	1533.677	62.646	2.8257	1514.012	23.218	6.1911	1511.004	38.496	6.4623	1510.485	31.13	4.5786
1556.406	49.892	0.3529	1576.894	63.849	0.1966	1531.579	21.638	6.2948	1536.076	41.11	10.7264	1528.2	29.772	4.9853
1588.88	49.229	0.0024	1611.909	65.445	0.7133	1546.657	23.799	7.2858	1555.055	43.421	2.7797	1545.917	31.524	7.5686
1603.074	49.115	1.519	1644.688	55.403	3.7068	1570.711	33.315	4.5493	1594.194	49.016	7.0204	1575.55	38.232	4.3931
1640.722	37.776	2.0096	1700.087	63.467	0.3296	1607.181	42.815	9.0204	1627.511	37.511	12.9508	1613.556	44.197	6.9779
1654.765	51.837	3.971	–	–	–	1633.809	36.347	16.5035	1649.373	33.977	13.2497	1639.679	38.677	15.963
1687.707	49.037	0.2147	–	–	–	1654.503	32.521	11.6542	1675.208	32.95	3.87	1654.653	34.479	7.3391
–	–	–	–	–	–	1679.157	27.622	2.9269	–	–	–	1679.511	34.993	4.3604

Graphs of the parentage area of the amide I sub-bands, summarizing the total β-structure, random coil and alpha-helix content in rat hippocampal tissue at both tested time intervals are showed in Fig. 3(a, b). σ-helix protein structure is absent in 42d for all groups; the predominant protein secondary structure is random coil and in lower amount β-sheet at two different frequencies as seen in Table 1. Meanwhile, σ-helix structure is strongly present in all groups at different amounts after 65d and is completely absent in AD group. The majority protein structure in AD group is random coil (the band centred at1642 cm-1 and a very little percentage of antiparallel β-sheet at 1694 cm-1. From [Table 1 & fig. 3], at early stage of Al intoxication (42d), the formation of both extracellular soluble random coil and parallel β-sheets structure is evident by the noticeable increase in the /The detected increase in the random coil sub-bands in AD1 and AD2 peak resolved may also suggests another second transit phase through random coil structure as our and other

previous works stated [3,5,10,12]. These findings are supported by the drastic increase in the sub-bands The slight observed increase in the HBW of the random coil of the β-protein sub-bands around 1640 cm-1 in AD1 group at 42d may be attributed to the fact that; the protein misfolding is a slow process that takes place through intermediate/or transit phase, which needs to break the hydrogen bonds and /or the reduction of the β-strand length, and hence proteins denaturation/ misfolding takes place [4,5,52,54]. The previous transit phase assumption of misfolded protein through β-sheets structure [subband at 1621 cm-1] in AD1 group holds true for the renaturation of protein in Cur group after 65d of treatment, which predominantly occurs through β-sheets structure but in this time accompanied with marked band shift to higher frequencies at 1633, 1627 cm-1 in Cur1 and Cur2 after 65d respectively]. These results consistent with that reported earlier[[1,8,14,15] which stated that nearly 90% of Aβ (40 amino acids) represents the soluble extracellular form while, 10% of Aβ (42) represents the hard intracellular hydrophobic core of Aβ form or NFTs. In this study, 91% of the amide I protein present in AD hippocampal tissue at 65d is random coil (the soluble extracellular protein) and 9% is antiparallel β-sheets structure which now represents the hard intracellular hydrophobic core of NFTs. The more neurotoxic protein structure that is associated with AD is believed to be the soluble extracellular Aβ that begin and continuously formed at the early stage of the disease pathogenesis and progression rather than tau proteins/NFTs in human, mice and rat brains [55]. The drastic benefit of utilizing SFTIRM over the conventional FTIR on following the protein aggregation is that how the secondary structure of protein in AD group is restricted exactly to two entities; random coil and antiparallel β-sheets represented by only two sub-bands at 1642 & 1694 cm-1 respectively, as the literatures compared to our previous studies [3,4] that gives several sub-bands for also rat hippocampal brain tissue.

3.2. Ratio measurements/ biomarkers

Fig. 2 (a-f) showed the above marked contribution of β-sheet, random coil and could be summarized the selected percentage area ratios and the total % area of σ-helix, β-sheet and random coil as follows.

i- Total percentage area of σ-helix, β-structure, and random coil after 42d and 65d in all tested groups; is an indicator of what kind of protein is there and how much (Fig. 2(a, b)) ii- β-sheet/ Random coil represented by % area 1640-1/1669cm-1 & 1640/1687; is an indicator/biomarker for the transformation, [through transit phase between these proteins secondary structure during both Al and LS treatments after 42d and 65d (Fig. 2(c, d)).

iii- Amide I/Amide II is used as an indicator of the change composition of the protein pattern; the changes in the protein secondary structure folding and unfolding (Fig. 2(e, f)). [44].

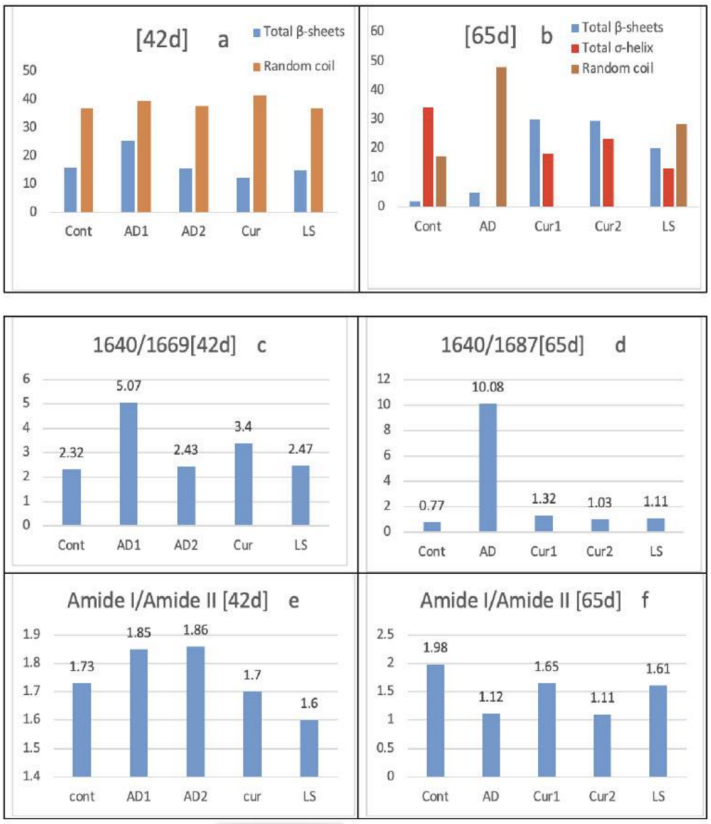

Figure 2. (a) Percentage area of total β-sheets and random coil at 42 days. (b) Percentage area of total β-sheets, random coil, and α-helix within the amide I secondary structure at 65 days in the four tested groups. A complete absence of α-helix structure is observed in the AD group, while random coil components disappear in the Cont and LS-treated groups at 65 days. (c) The role of β-turn as a transitional phase in Aβ transformation in AD at 42 days. (d) Contribution of β-sheet to protein renaturation after 65 days. (e) Variations in the total amide I/amide II ratios at 42 days and (f) at 65 days.

3.3. SFTIRM mapping

The protein profile of all tested groups at 42d and 65d are showed in Fig 3 and were obtained by the peak around 1657 cm-1. It seems that at early stage of either AL and LS induction, there are great activities in protein misfolding/refolding as mentioned above and SFTIRM, our previous reports [3,5,14,16]are also supporting these results.In order to validate and monitor the difference in biochemical structure of the control, Alinduced AD like and other tested groups in brain cortical tissue, we divided the IR spectra into three distinct regions namely; the membrane lipids and fatty acids of CH stretching over 30202810 cm-1, the amide I and amide II of C=O stretching and N-H bending of proteins respectively over 1700-1500 cm-1, and the Phosphate & nucleic acids1300-900 cm-1 regions. Here in this work, we only focused on the amide region over 1700-1500 cm-1. The other regions will be discussed later in another work.

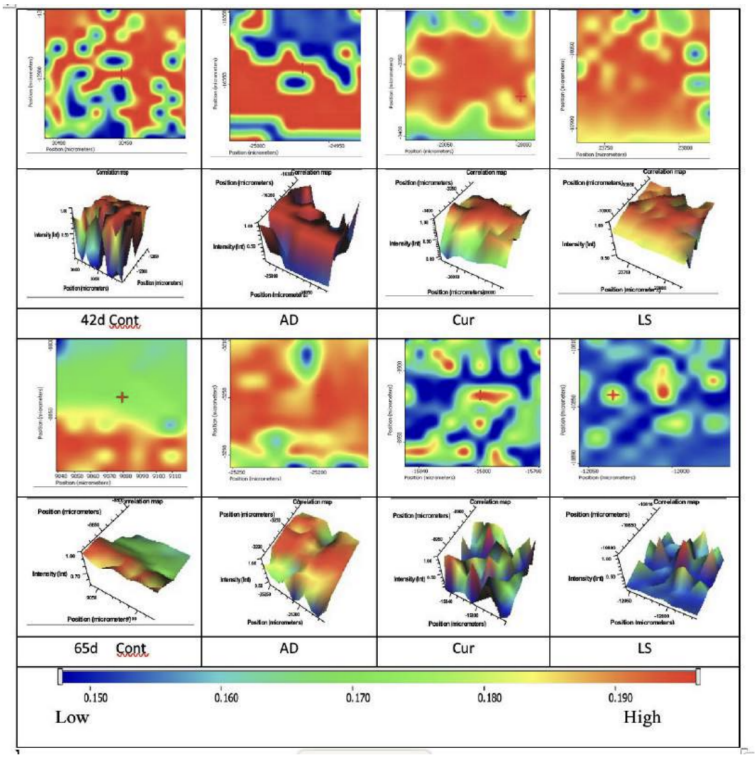

Figure 3. SFTIRM profile of hippocampal protein (amide I) showing distinct differences in protein distribution and intensity among Cont, AD, Cur, and LS groups. LS-treated groups (Cur and LS) displayed comparable protein distribution at both 42 and 65 days, whereas the AD group exhibited markedly different and denser protein distribution relative to Cont and LS-treated groups at both time points. The colour bar represents protein levels from low (blue) to high (red). The scanned region was acquired at 10 μm steps using a 40 $\times$ 40 μm aperture.

3.4. Multivariate analysis

In order to validate and monitor the difference in biochemical structure of the control, Alinduced AD like and other tested groups in brain cortical tissue, we divided the IR spectra into three distinct regions namely; the membrane lipids and fatty acids of CH stretching over 30202810 cm-1, the amide I and amide II of C=O stretching and N-H bending of proteins respectively over 1700-1500 cm-1, and the Phosphate & nucleic acids1300-900 cm-1 regions. Here in this work, we only focused on the amide region over 1700-1500 cm-1. The other regions will be discussed later in another work.

4. Statistical analysis

We used both HCA and PCA multivariate analysis, over the amide I and amide II bands (17001500 cm 1) of rat brain hippocampal tissues, to monitor how significantly the biochemical spectra among groups are different. These analyses were performed on the already processed sFTIRM spectra obtained of the absorbed amide I and amide II band's intensities. Fig. 4(a) showed that, after 42d of treatment, both HCA and PCA could not differentiate between Cont and AD groups, at the same time, they clustered proteins for AD group into two entities. It seems that the proteins have two different secondary structure at the early stage of disease (42d), it fluctuated still between normal and misfolded types, in AD model, indicated by the higher heterogeneity between the two clustered groups of in HCA; greater than 430 [black arrow (zone of interference (brown arrow)].

Meanwhile, HCA and PCA between Cur and AD groups succeeded partially to differentiate between these groups over the same time of treatment Figure 4. On the other hand, for longer time of treatment after 65d, HCA and PCA between Cont and AD

groups showed a significant and a complete segregation Figure 4. The same complete segregation between the Cur and the AD groups are shown after 65d Figure 4. At the late stage of induced AD-like model after 65d, both Cont and AD groups established [obtained] their own protein secondary structure each of their main form and hence, HCA & PCA succeeded completely to segregate between them. Meanwhile, Cur group is the one that shows now two main protein secondary structures as the recovery and reversing the process of misfolding is not completed yet at that time of the experiment Fig. 4(d) black arrows (zone of interference (brown arrow)

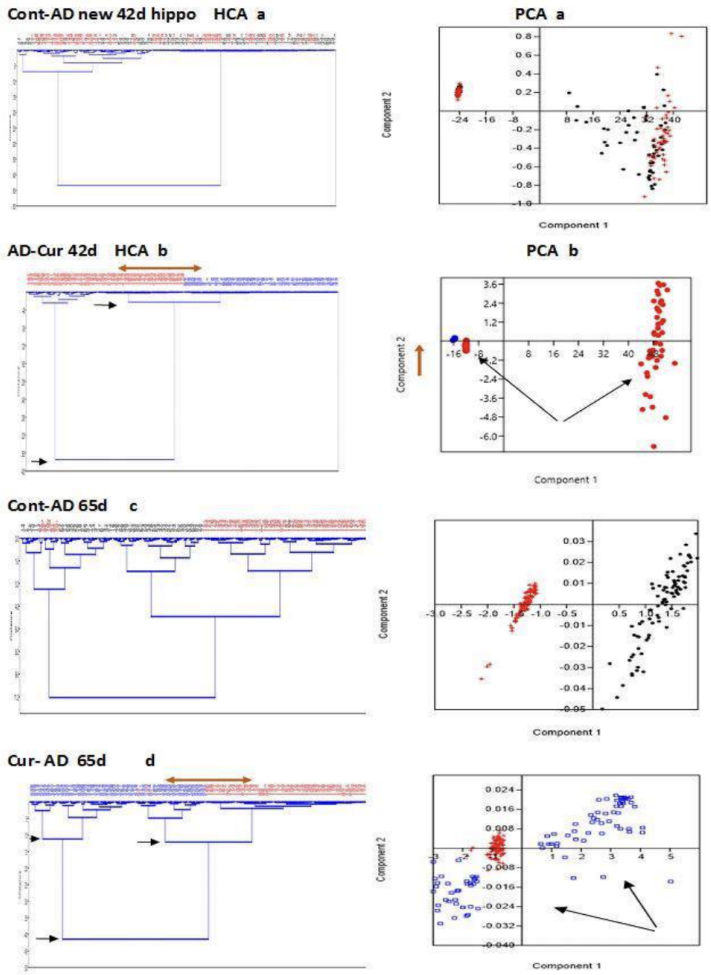

Figure 4. HCA and PCA outcomes following Al induction. (a) At 42 days, HCA and PCA failed to discriminate between Cont and AD groups. (b) However, partial segregation was observed between AD and Cur groups after LS treatment, with a zone of interference indicated by brown arrows. The heterogeneity value between Cur and AD at 42 days exceeded 460, while fluctuations in the interference region were below 20. PCA also indicated the presence of two distinct amide populations within the AD group at this stage. (c) At 65 days, HCA and PCA successfully differentiated Cont from AD. In contrast, multivariate analysis only partially segregated AD from Cur groups at the same time point. The Cur group exhibited two distinct protein entities, whereas Cont and AD groups did not.

5. Conclusion

To conclude, Al can induce AD and trigger amyloidosis that happens through slow intermediate/or transit phase. At early stage (42d) AD protein misfolding takes place through two pass ways; mainly random coil and with little contribution β-turn structure. SFTIRM detected precisely, much better than the conventional FTIR, both types of Aβ;

soluble extracellular and insoluble intracellular forms at 65d. On the other hand, the process of refolding the proteins and reversing Al effects in response to LS treatment occurs through only β-structure transit phase at 42d & 65d. -helix structure is completely absent in only AD group at the end of experiment after 65d.

Author contribution declaration

Safaa K.H. Khalil: Conceptualization, Methodology, Investigation, Formal analysis, Resources, Writing draft, Writing - review & editing, W. El Hotaby: Investigation, Formal analysis, Resources, Writing draft, Writing review & editing, Gehan A.-R. Ahmed: Conceptualization and Design of the study, Methodology, Investigation, Formal analysis, Resources, Writing - original draft, Writing – review & editing, Gihan Kamel: Investigation, Writing – draft, Hadeer H.A. Sherif: Investigation, Resources, Lamyaa Abbas: Investigation, Formal analysis, Resources, Writing draft, Writing review & editing

Statements and Declarations

The authors declare that they have no known competing financial interests or personal relationships that could have appeared to influence the work reported in this paper.

Funding

This work is partially supported by National Research Centre, Giza, Egypt. All SFTIRM measurements were covered and conducted at Synchrotron light for Experimental Science and Applications in the Middle East (SESAME), Jordan

Conflict of Interest

All authors confirm that there is no conflict of interest.

Data Availability

All data generated or analysed during this study are included in this published article (and its Supplementary Information files).

References

1. Ball, M.J. Neuronal loss, neurofibrillary tangles and granulovacuolar degeneration in the hippocampus with ageing and dementia. A quantitative study. *Acta Neuropathol.* **1977**, 37, 111–118. [Google Scholar] [PubMed]
2. Miller, L.M.; Bourassa, M.W.; Smith, R.J. FTIR spectroscopic imaging of protein aggregation in living cells. *Biochim. Biophys. Acta* **2013**, 1828, 2339–2346. [Google Scholar] [PubMed]
3. Ahmed, G.A.R.; el Hotaby, W.; Abbas, L.; Sherif, H.H.A.; Kamel, G.; Khalil, S.K.H. Synchrotron Fourier transform infrared microspectroscopy (sFTIRM) analysis of Al-induced Alzheimer's disease in rat brain cortical tissue. *Spectrochim. Acta A Mol. Biomol. Spectrosc.* **2020**, 239. [Google Scholar] [PubMed]
4. Balgoon, M.J.; Ahmed, G.A.R.; Qusti, S.Y.; Shaker, S. Transit phases of -amyloid and tau proteins formation and resolubilisation in AD rat hippocampus tissue as probed by ATR-IR spectroscopy. *Neurol. Psychiatry Brain Res.* **2019**, 31, 1–8. [Google Scholar] [PubMed]
5. Balgoon, M.J.; Ahmed, G.A.R.; Qusti, S.Y. FT-Raman study of protein misfolding and renaturation in brain hippocampus. *Neurol. Psychiatry Brain Res.* **2018**, 30, 101–109. [Google Scholar] [PubMed]
6. Ahmed, G.A.R.; El Hotaby, W.; Abbas, L.; Sherif, H.H.A.; Kamel, G.; Khalil, S.K.H. Synchrotron Fourier transform infrared microspectroscopy (sFTIRM) analysis of Al-induced Alzheimer's disease in rat brain cortical tissue. *Spectrochim. Acta A Mol. Biomol. Spectrosc.* **2020**, 239. [Google Scholar] [PubMed]
7. Schultzberg, M.; Lindberg, C.; Aronsson, Å.F.; Hjorth, E.; Spulber, S.D.; Oprica, M. Inflammation in the nervous system–physiological and pathophysiological aspects. *Physiol. Behav.* **2007**, 92, 121–128. [Google Scholar] [PubMed]
8. Miller, L.M.; Bourassa, M.W.; Smith, R.J. FTIR spectroscopic imaging of protein aggregation in living cells. *Biochim. Biophys. Acta* **2013**, 1828, 2339. [Google Scholar] [PubMed]

9. Walsh, D.M.; Minogue, A.M.; Sala Frigerio, C.; Fadeeva, J.V.; Wasco, W.; Selkoe, D.J. The APP family of proteins: similarities and differences. *Biochem. Soc. Trans.* **2007**, 35, 416–420. [Google Scholar] [PubMed]
10. Korte, M.; Herrmann, U.; Zhang, X.; Draguhn, A. The role of APP and APLP for synaptic transmission, plasticity, and network function: lessons from genetic mouse models. *Exp. Brain Res.* **2012**, 217, 435–440. [Google Scholar] [PubMed]
11. Haass, C.; Kaether, C.; Thinakaran, G.; Sisodia, S. Trafficking and proteolytic processing of APP. *Cold Spring Harb. Perspect. Med.* **2012**, 2. [Google Scholar] [PubMed]
12. Ii, K. The role of beta-amyloid in the development of Alzheimer's disease. *Drugs Aging* **1995**, 7, 97–109. [Google Scholar] [PubMed]
13. Kawahara, M.; Kato-Negishi, M. Link between Aluminum and the Pathogenesis of Alzheimer's Disease: The Integration of the Aluminum and Amyloid Cascade Hypotheses. *Int. J. Alzheimers Dis.* **2011**, 2011. [Google Scholar] [PubMed]
14. A-R Ahmed, G.; Khalil, S.K.H.; el hotaby, W.; Abbas, L.; Sherif, H.H.A.; Abdel-Rahman, E.A.; et al. ATR-IR and EPR spectroscopy for detecting the alterations in cortical synaptosomes induced by aluminium stress. *Spectrochim. Acta A Mol. Biomol. Spectrosc.* **2020**, 228, 117535. [Google Scholar] [PubMed]
15. Kang, J.; Lemaire, H.G.; Unterbeck, A.; Salbaum, J.M.; Masters, C.L.; Grzeschik, K.H.; et al. The precursor of Alzheimer's disease amyloid A4 protein resembles a cell-surface receptor. *Nature* **1987**, 325, 733–736. [Google Scholar] [PubMed]
16. Ahmed, G.A.R.; Khalil, S.K.H.; Hotaby, W el; Abbas, L.; Farrag, A.R.H.; Aal, W.E.A.; et al. ATR-IR and EPR spectroscopy for following the membrane restoration of isolated cortical synaptosomes in aluminium-induced Alzheimer's disease - Like rat model. *Chem. Phys. Lipids* **2020**, 231. [Google Scholar] [PubMed]
17. Bulck, M. Van; Sierra-Magro, A.; Alarcon-Gil, J.; Perez-Castillo, A.; Morales-Garcia, J.A. Novel Approaches for the Treatment of Alzheimer's and Parkinson's Disease. *Int. J. Mol. Sci.* **2019**, 20. [Google Scholar] [PubMed]
18. Benedikz, E.; Kloskowska, E.; Winblad, B. The rat as an animal model of Alzheimer's disease. *J. Cell Mol. Med.* **2009**, 13, 1034–1042. [Google Scholar] [PubMed]
19. Liao, C.R.; Rak, M.; Lund, J.; Unger, M.; Platt, E.; Albensi, B.C.; et al. Synchrotron FTIR reveals lipid around and within amyloid plaques in transgenic mice and Alzheimer's disease brain. *Analyst* **2013**, 138, 3991–3997. [Google Scholar] [PubMed]
20. Lecanu, L.; Papadopoulos, V. Modeling Alzheimer's disease with non-transgenic rat models. *Alzheimers Res. Ther.* **2013**, 5. [Google Scholar] [PubMed]
21. Eddouks, M.; Maghrani, M.; Zeggwagh, N.A.; Michel, J.B. Study of the hypoglycaemic activity of Lepidium sativum L. aqueous extract in normal and diabetic rats. *J. Ethnopharmacol.* **2005**, 97, 391–395. [Google Scholar] [PubMed]
22. Maghrani, M.; Zeggwagh, N.A.; Michel, J.B.; Eddouks, M. Antihypertensive effect of Lepidium sativum L. in spontaneously hypertensive rats. *J. Ethnopharmacol.* **2005**, 100, 193–197. [Google Scholar] [PubMed]
23. Balgoon, M.J.; Ahmed, G.A.R.; Qusti, S.Y.; Shaker, S. Transit phases of -amyloid and tau proteins formation and re-solubilisation in AD rat hippocampus tissue as probed by ATR-IR spectroscopy. *Neurol. Psychiatry Brain Res.* **2019**, 31, 1–8. [Google Scholar] [PubMed]
24. Di, J.; Yao, K.; Han, W.; Bi, S. Study on the interaction of copper-zinc superoxide dismutase with aluminum ions by electrochemical and fluorescent method. *Spectrochim. Acta A Mol. Biomol. Spectrosc.* **2006**, 65, 896–900. [Google Scholar] [PubMed]
25. Turker, S.; Severcan, M.; Ilbay, G.; Severcan, F. Epileptic seizures induce structural and functional alterations on brain tissue membranes. *Biochim. Biophys. Acta (BBA) - Biomembranes* **2014**, 1838, 3088–3096. [Google Scholar] [PubMed]
26. Jurkić, L.M.; Cepanec, I.; Pavelić, S.K.; Pavelić, K. Biological and therapeutic effects of ortho-silicic acid and some ortho-silicic acid-releasing compounds: New perspectives for therapy. *Nutr. Metab. (Lond).* **2013**, 10. [Google Scholar] [PubMed]
27. Dong, J.; Atwood, C.S.; Anderson, V.E.; Siedlak, S.L.; Smith, M.A.; Perry, G.; et al. Metal binding and oxidation of amyloid-beta within isolated senile plaque cores: Raman microscopic evidence. *Biochemistry* **2003**, 42, 2768–2773. [Google Scholar] [PubMed]
28. Nićiforović, N.; Abramovič, H. Sinapic Acid and Its Derivatives: Natural Sources and Bioactivity. *Compr. Rev. Food Sci. Food Saf.* **2014**, 13, 34–51. [Google Scholar] [PubMed]
29. Raouf, G.A.; Gashlan, H.M.; Khedr, A.; Hamedy, S.; Al-jabbri, H. IN VITRO NEW BIOPOLYMER FOR BONE GRAFTING AND BONE CEMENT. *2018*. [Google Scholar] [PubMed]
30. Williams, G.P.; Duncan, W.D. Infrared synchrotron radiation from electron storage rings. *Appl. Opt.* **1983**, 22, 2914–2923. [Google Scholar] [PubMed]
31. Cheng, J.X.; Xie, X.S. Vibrational spectroscopic imaging of living systems: An emerging platform for biology and medicine. *Science* **2015**, 350. [Google Scholar] [PubMed]
32. Fändrich, M. On the structural definition of amyloid fibrils and other polypeptide aggregates. *Cell Mol. Life Sci.* **2007**, 64, 2066–2078. [Google Scholar] [PubMed]
33. Liao, C.R.; Rak, M.; Lund, J.; Unger, M.; Platt, E.; Albensi, B.C.; et al. Synchrotron FTIR reveals lipid around and within amyloid plaques in transgenic mice and Alzheimer's disease brain. *Analyst* **2013**, 138, 3991–3997. [Google Scholar] [PubMed]
34. Carr, G.L.; Reffner, J.A.; Williams, G.P. Performance of an infrared microspectrometer at the NSLS. *Rev. Sci. Instrum.* **1998**, 66, 1490. [Google Scholar] [PubMed]

35. Reffner, J.A.; Martoglio, P.A.; Williams, G.P. Fourier transform infrared microscopical analysis with synchrotron radiation: The microscope optics and system performance (invited). *Rev. Sci. Instrum.* **1998**, 66, 1298. [Google Scholar] [PubMed]
36. Sharma, S.; Agarwal, N. Nourishing and healing prowess of garden cress (Lepidium sativum Linn.) A review. *Indian J. Nat. Prod. Resour.* **2011**, 2, 292–297. [Google Scholar] [PubMed]
37. Eddouks, M.; Maghrani, M.; Zeggwagh, N.A.; Michel, J.B. Study of the hypoglycaemic activity of Lepidium sativum L. aqueous extract in normal and diabetic rats. *J. Ethnopharmacol.* **2005**, 97, 391–395. [Google Scholar] [PubMed]
38. Baker, M.J.; Trevisan, J.; Bassan, P.; Bhargava, R.; Butler, H.J.; Dorling, K.M.; et al. Using Fourier transform IR spectroscopy to analyze biological materials. *Nat. Protoc.* **2014**, 9, 1771–1791. [Google Scholar] [PubMed]
39. Yonar, D.; Ocek, L.; Tiftikcioglu, B.I.; Zorlu, Y.; Severcan, F. Relapsing-Remitting Multiple Sclerosis diagnosis from cerebrospinal fluids via Fourier transform infrared spectroscopy coupled with multivariate analysis. *Sci. Rep.* **2018**, 8. [Google Scholar] [PubMed]
40. Turker, S.; Severcan, M.; Ilbay, G.; Severcan, F. Epileptic seizures induce structural and functional alterations on brain tissue membranes. *Biochim. Biophys. Acta* **2014**, 1838, 3088–3096. [Google Scholar] [PubMed]
41. Rak, M.; Del Bigio, M.R.; Mai, S.; Westaway, D.; Gough, K.M. Dense-core and diffuse Abeta plaques in TgCRND8 mice studied with synchrotron FTIR microspectroscopy. *Biopolymers* **2007**, 87, 207–217. [Google Scholar] [PubMed]
42. Kuzyk, A.; Kastyak, M.; Agrawal, V.; Gallant, M.; Sivakumar, G.; Rak, M.; et al. Association among Amyloid Plaque, Lipid, and Creatine in Hippocampus of TgCRND8 Mouse Model for Alzheimer Disease. *J. Biol. Chem.* **2010**, 285, 31202. [Google Scholar] [PubMed]
43. Kastyak-Ibrahim, M.Z.; Nasse, M.J.; Rak, M.; Hirschmugl, C.; Del Bigio, M.R.; Albensi, B.C.; et al. Biochemical labelfree tissue imaging with subcellular-resolution synchrotron FTIR with focal plane array detector. *Neuroimage* **2012**, 60, 376–383. [Google Scholar] [PubMed]
44. Saeed, A.; Raouf, G.A.; Nafee, S.S.; Shaheen, S.A.; Al-Hadeethi, Y. Effects of Very Low Dose Fast Neutrons on Cell Membrane And Secondary Protein Structure in Rat Erythrocytes. *PLoS One* **2015**, 10, e0139854. [Google Scholar] [PubMed]
45. Liao, C.R.; Rak, M.; Lund, J.; Unger, M.; Platt, E.; Albensi, B.C.; et al. Synchrotron FTIR reveals lipid around and within amyloid plaques in transgenic mice and Alzheimer's disease brain. *Analyst* **2013**, 138, 3991–3997. [Google Scholar] [PubMed]
46. De Meutter, J.; Goormaghtigh, E. Evaluation of protein secondary structure from FTIR spectra improved after partial deuteration. *Eur. Biophys. J.* **2021**, 50, 613–628. [Google Scholar] [PubMed]
47. Byler, D.M.; Susi, H. Examination of the secondary structure of proteins by deconvolved FTIR spectra. *Biopolymers* **1986**, 25, 469–487. [Google Scholar] [PubMed]
48. Kastyak-Ibrahim, M.Z.; Nasse, M.J.; Rak, M.; Hirschmugl, C.; Del Bigio, M.R.; Albensi, B.C.; et al. Biochemical labelfree tissue imaging with subcellular-resolution synchrotron FTIR with focal plane array detector. *Neuroimage* **2012**, 60, 376–383. [Google Scholar] [PubMed]
49. Miller, L.M.; Wang, Q.; Telivala, T.P.; Smith, R.J.; Lanzirotti, A.; Miklossy, J. Synchrotron-based infrared and X-ray imaging shows focalized accumulation of Cu and Zn co-localized with beta-amyloid deposits in Alzheimer's disease. *J. Struct. Biol.* **2006**, 155, 30–37. [Google Scholar] [PubMed]
50. Berriman, J.; Serpell, L.C.; Oberg, K.A.; Fink, A.L.; Goedert, M.; Crowther, R.A. Tau filaments from human brain and from in vitro assembly of recombinant protein show cross- structure. *Proc. Natl. Acad. Sci. U S A* **2003**, 100, 9034–9038. [Google Scholar] [PubMed]
51. Barghorn, S.; Davies, P.; Mandelkow, E. Tau paired helical filaments from Alzheimer's disease brain and assembled in vitro are based on beta-structure in the core domain. *Biochemistry* **2004**, 43, 1694–1703. [Google Scholar] [PubMed]
52. Hilpert, H.; Guba, W.; Woltering, T.J.; Wostl, W.; Pinard, E.; Mauser, H.; et al. -secretase (BACE1) inhibitors with high in vivo efficacy suitable for clinical evaluation in Alzheimer's disease. *J. Med. Chem.* **2013**, 56, 3980–3995. [Google Scholar] [PubMed]
53. Axelsen, P.H.; Komatsu, H.; Murray, I.V.J. Oxidative stress and cell membranes in the pathogenesis of Alzheimer's disease. *Physiology (Bethesda)* **2011**, 26, 54–69. [Google Scholar] [PubMed]
54. Cerf, E.; Sarroukh, R.; Tamamizu-Kato, S.; Breydo, L.; Derclayes, S.; Dufrênes, Y.F.; et al. Antiparallel -sheet: a signature structure of the oligomeric amyloid -peptide. *Biochem. J.* **2009**, 421, 415–423. [Google Scholar] [PubMed]
55. Cleary, J.P.; Walsh, D.M.; Hofmeister, J.J.; Shankar, G.M.; Kuskowski, M.A.; Selkoe, D.J.; et al. Natural oligomers of the amyloid-beta protein specifically disrupt cognitive function. *Nat. Neurosci.* **2005**, 8, 79–84. [Google Scholar] [PubMed]